Pergamon

Int. J. Heat Mass Transfer. Vol. 40, No. 2. pp. 323–332, 1997

0017–9310/97 $15.00 + 0.00

PII: S0017-9310(96)00103-2

Radiative exchange between a cylindrical crystal and a monoellipsoidal mirror furnace

RODRIGO HAYA, DAMIÁN RIVAS† and JAVIER SANZ

Lamf, E.T.S.I. Aeronáuticos, Universidad Politécnica de Madrid, 28040 Madrid, Spain

(*Received* 14 *September* 1995 *and in final form* 12 *March* 1996)

Abstract—The heating of a cylindrical sample in a monoellipsoidal mirror furnace is considered. A radiation model is formulated for slender samples where the radiative exchange between the sample and the mirror is studied analytically. To analyse the behavior of the model, the temperature field in the sample is calculated using a one-dimensional conduction–radiation model. The differences with respect to a model where the radiative exchange is not considered are not only quantitative but qualitative. The model predicts a strongly asymmetric heating, which may cause asymmetries in the grown crystal as observed experimentally. Comparison with experimental data is made. Copyright © 1996 Elsevier Science Ltd.

1. INTRODUCTION

The availability of the microgravity environment for crystal growth has given rise to the use of mirror heating facilities for non-intrusive melting, in particular ellipsoidal mirror furnaces, where the radiation from halogen lamps is focused by the mirror on the sample [1]. In this paper we consider a monoellipsoidal furnace, which consists of an ellipsoidal mirror where the lamp is placed in one focus and the sample in the other. This type of furnace has the advantage of providing axisymmetrical irradiation onto the sample (double-ellipsoid furnaces and other many-lobuled geometries also tried do not share this rotational symmetry). The irradiation profile on the surface of the sample can be obtained as an explicit function of the physical parameters that appear in the problem [2]. This type of furnaces is widely used in the floating zone technique for crystal growth [3–5] (it has been used also for Czochralski growth [6]).

In ref. [2] the heating of a cylindrical sample was studied in a model where the redistribution by the mirror of the radiation losses from the sample was not included. In the present work we reformulate the model so that that effect is taken into account: the energy radiated by the sample is reflected by the mirror and redistributed along the sample [7, 8]. We will call this model the reflection model, as opposed to the non-reflection model where the radiative exchange between sample and furnace is not considered; in this latter model, the mirror has the only effect of reflecting the energy emitted by the lamp, thus, the radiation from the sample is just lost. In the formulation of the radiative exchange, the determination of the view factor between different points on the sample is carried out.

In our formulation we take advantage of the fact that for slender samples the temperature field is practically unidimensional [2]: in the radiation problem the sample will be considered one-dimensional (1D) and, in order to analyse the behavior of the radiation model, the temperature field in the sample will be calculated using a simplified 1D model. The results show that the temperature field changes not only quantitatively but qualitatively when the reflection at the mirror of the radiation from the sample is taken into account. To the best of our knowledge this is the first work related to the floating zone technique in ellipsoidal furnaces where the radiative exchange between mirror and sample is studied analytically. Other thermal models for crystal growth in the floating zone configuration have been made by different authors [9–11], but they consider a circumferential heater around the sample, and not a mirror furnace.

Our interest in this paper is to get insight into the radiation problem, thus, for simplicity, the physical properties of the material will be assumed constant. In the floating zone technique the rod is slowly pulled out so that the molten region travels along it. In this paper the effect of pulling is not considered either, although results for different positionings of the sample are presented (these results will provide an approximate quasi-stationary description of the actual pulling process). Obviously only slender samples are considered in this work (which is the case in practice [12]). Results for a silicon sample are presented, and comparison with experiments is made. The agreement between the results obtained with the reflection model and the experimental data is quite good.

2. FURNACE GEOMETRY AND IRRADIATION PROFILES

In this section the irradiation profile on the sample generated by the furnace is obtained (see [2] for more

† Author to whom correspondence should be addressed.

NOMENCLATURE

a, b	semiaxes of the ellipsoid
B	radiosity
d	distance between the center of the sample and the focus
e	eccentricity of the elliptic section
F	view factor
H	net incident radiation
I, I'	radiation and reflected radiation intensity
K	view factor kernel
L	half the length of the sample
p	parameter of the elliptic section
P_W	dimensionless power parameter
q	dimensionless heat flux
Q	heat flux
r	sample radial coordinate
R	radius of the sample
Ra	dimensionless radiation parameter
T	temperature
T_m	melting temperature
W_L	lamp power
z	sample and ellipsoid axial coordinate
Z_m	molten zone length.

Greek symbols

α	absorptance
ε	emissivity
η	ellipsoid axial coordinate
θ	dimensionless temperature and angle in the furnace geometry
κ	thermal conductivity
Λ	slenderness of the sample
ξ, ξ'	distance point-focus
ξ_1, ξ_2	distances from a point of the ellipsoid to the foci
ρ	reflectance
σ	Stefan–Boltzmann constant
ϕ	angle in the furnace geometry.

Subscripts

b	upper base of the sample
i	element i
j	element j
L	lateral surface of the sample
0	reference value
max	maximum value
top	upper base of the sample.

Superscripts

^	dimensional value
~	dimensional value
¯	average value.

details). The shape of the furnace is an ellipsoid of revolution of semiaxes a and b, as shown in Fig. 1. The distances from the two foci to a point of the ellipse, ξ_1 and ξ_2, are given by

$$\xi_1 = \frac{p}{1-e\cos\theta} \quad \xi_2 = \frac{p}{1+e\cos\phi} \tag{1}$$

with $\xi_1+\xi_2 = 2a$, and where $p = b^2/a$, $e = \sqrt{1-(b/a)^2}$ and θ and ϕ are defined in Fig. 1(a).

The lamp is supposed to be a point source placed in one of the foci of the ellipsoid. The influence of the out-of-focus position of the lamp on the temperature field is studied in [1, 13]. The sample is cylindrical of length $2L$ and radius R and it is placed on the other focus, with its axis of revolution along the axis of revolution of the ellipsoid. The center of the cylinder may be displaced some distance $\hat{d}$ with respect to the focus, as shown in Fig. 1(b).

The intensity of the radiation generated by the lamp in points at a distance ξ ($\xi < \xi_1$) from the focus is given by

$$\xi^2 I = \frac{1}{4\pi} W_L \tag{2}$$

where W_L is the power of the lamp. Here, the case of a lamp with isotropic radiation is considered. The ellipsoidal furnace surface is supposed to be a perfect mirror within the approximation of geometrical optics. Hence, for the intensity of the reflected radiation, I', at a distance ξ' ($\xi' < \xi_2$) from focus F' one has

$$I' = \left(\frac{\xi_2}{\xi_1}\right)^2 \frac{W_L}{4\pi\xi'^2}. \tag{3}$$

The lateral surface of the cylinder is defined by $\xi'_L = R/\sin\phi$, thus, the heat flux on this surface (absorbed radiation) is given by

$$Q = \alpha I'(\xi'_L)\sin\phi = \frac{\alpha W_L}{4\pi R^2} \frac{\sin^3\phi}{\left[\frac{2a}{p}(1+e\cos\phi)-1\right]^2} \tag{4}$$

where $\alpha = \varepsilon$ is the absorptance of the sample (considered as a gray body). If we adopt now a cylindrical coordinate system, coordinates $\hat{r}$ and $\hat{z}$ as shown in Fig. 1(b), we have $\tan\phi = R/(\hat{z}-\hat{d}) = 1/(\Lambda(z-d))$, where $z = \hat{z}/L$ is the dimensionless longitudinal coordinate, $d = \hat{d}/L$ is the dimensionless center displacement and $\Lambda = L/R$ is the slenderness of the sample. Thus, if we write $Q = Q_0 q(z)$, with

$$Q_0 = \frac{\alpha W_L}{4\pi R^2} \tag{5}$$

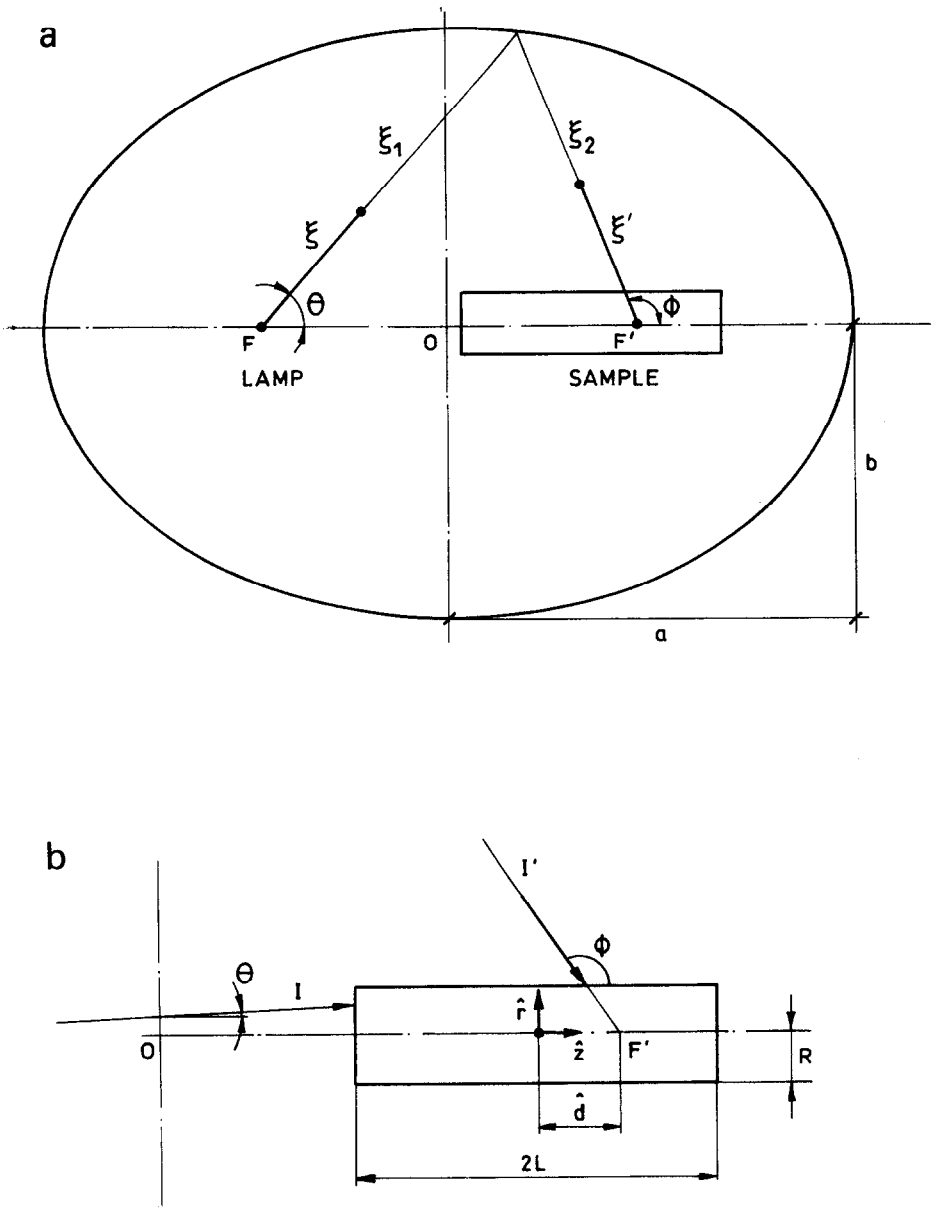

Fig. 1. (a) Geometry of the furnace; (b) geometry of the sample.

we obtain the following dimensionless irradiation profile

$$q(z) = (1+\Lambda^2(z-d)^2)^{-3/2}\left[\frac{2}{1-e^2} \times\left(1+\frac{e\Lambda(z-d)}{\sqrt{1+\Lambda^2(z-d)^2}}\right)-1\right]^{-2} \quad (6)$$

which is plotted in [2] for $d = 0$ and several values of Λ and b/a.

Next the irradiation profile on the upper base of the cylinder (the base closer to the lamp) is obtained. There are two different terms contributing to this profile: one Q_{b1}, the direct radiation from the lamp and, the other, Q_{b2}, the radiation that arrives to the base after being reflected by the mirror. The upper base of the cylinder is defined by $\xi_b = (2ea-(L+\hat{d}))/\cos\theta$, thus, the direct heat flux distribution on this surface is given by

$$Q_{b1} = \alpha I(\xi_b)\cos\theta = \frac{\alpha W_L}{4\pi L^2}\frac{\cos^3\theta}{\left(2e\frac{a}{L}-(1+d)\right)^2}. \quad (7)$$

If now we write $Q_{b1} = Q_o q_{b1}(r)$, we obtain for the dimensionless profile $q_{b1}(r)$ the following:

$$q_{b1}(r) = \frac{\Lambda\left(2e\frac{a}{L}-(1+d)\right)}{\left[r^2+\Lambda^2\left(2e\frac{a}{L}-(1+d)\right)^2\right]^{3/2}} \quad (8)$$

where $r = \hat{r}/R$ is the dimensionless radial coordinate in the system centered in the cylinder. The upper base of the cylinder is also defined by $\xi_b'^2 = \hat{r}^2 - (L+\hat{d})^2$, thus the radiation absorbed by this surface after being reflected at the mirror is

$$Q_{b2} = -\alpha I'(\xi_b')\cos\phi = -\frac{\alpha W_L}{4\pi R^2}\frac{1}{r^2+\Lambda^2(1+d)^2}\frac{\cos\phi}{\left[\frac{2a}{p}(1+e\cos\phi)-1\right]^2}. \quad (9)$$

The relationship between r and ϕ (at the upper base) is given by

$$\cos\phi = \frac{-\Lambda(1+d)}{\sqrt{r^2+\Lambda^2(1+d)^2}} \quad (10)$$

therefore if we write $Q_{b2} = Q_0 q_{b2}(r)$, we obtain

$$q_{b2}(r) = \frac{\Lambda(1+d)}{(r^2+\Lambda^2(1+d)^2)^{3/2}}\left[\frac{2}{1-e^2} \times\left(1-\frac{e\Lambda(1+d)}{\sqrt{r^2+\Lambda^2(1+d)^2}}\right)-1\right]^{-2}. \quad (11)$$

The profile $q_{b1}(r)+q_{b2}(r)$ turns out to be much weaker than the profile $q(z)$ obtained above: for $d = 0$, $\Lambda = 10$, $b/a = 0.9$, and $L/a = 0.5$, $(q_{b1}+q_{b2})_{max} \approx 0.076$, whereas $q_{max} \approx 0.76$.

3. RADIATIVE EXCHANGE BETWEEN SAMPLE AND MIRROR

A model based on the following postulates is adopted.

(1) All the surfaces are considered gray bodies.

(2) The sample is supposed to emit and reflect diffusely.

(3) The mirror is supposed to emit diffusely and reflect specularly.

(4) The sample is considered one-dimensional.

(5) The irradiation profile generated by the lamp acting on the 1D sample, $Q(z)$, is the one given by equations (5) and (6).

The interchange of energy among the different parts of the furnace is divided in the following manner (see Fig. 2):

Region 1. Part of the cylinder located to the left of focus F'.

Region 2. Part of the cylinder located to the right of focus F'.

Region 3. Lamp and any other surface inside the furnace.

In this way, region 2 interchanges energy only with region 3, and region 1 interchanges energy with regions 1 and 3. Only the interchange of energy 1–1 will be considered here. Furthermore, only one reflection at the mirror will be taken into account, thus any one ray leaving the sample which is reflected two or more times at the mirror is considered lost.

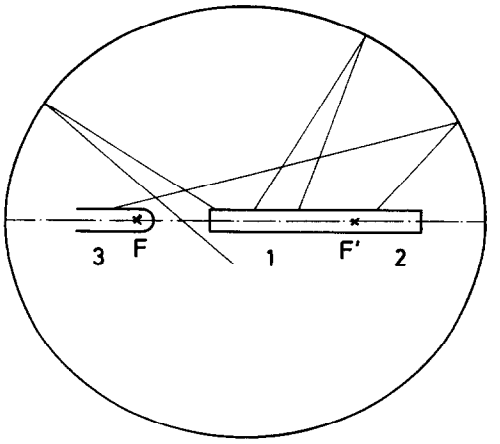

Fig. 2. Exchange of radiation inside the furnace.

Defining the radiosity of a surface element j as the radiant energy leaving the surface element (see [14]), one has

$$B_j = \varepsilon_j\sigma T_j^4 + \rho_j H_j \quad (12)$$

where $\rho_j = 1-\varepsilon_j$ and H_j is the net incident radiation on surface element j, which is given by

$$H_j = \sum_i B_i F_{j-i} \quad (13)$$

where F_{j-i} is the view factor between the surface elements i and j, namely the fraction of the radiant energy leaving surface element j that arrives at surface element i. The energy balance for surface element j provides

$$Q_{L_j} = \varepsilon_j\sigma T_j^4 - \alpha_j H_j - Q_j \quad (14)$$

where $\alpha_j = \varepsilon_j$ and Q_j is the irradiation profile generated by the lamp. In the previous energy balance, the radiation emitted by the mirror (which is at temperature T_0) is neglected (in practice $T_0 < 500$K and $\varepsilon_{500} \cong 0.2$). Rearranging the previous equations the following set of implicit equations is obtained

$$Q_{L_j} = \varepsilon_j\sigma T_j^4 - \varepsilon_j\sigma\sum_i T_i^4 F_{j-i} + \varepsilon_j\sum_i\frac{1-\varepsilon_i}{\varepsilon_i}Q_{L_i}F_{j-i} - Q_j. \quad (15)$$

If we consider differential surface elements, the following integral equation is obtained

$$Q_L(\tilde{z}) = \varepsilon(\tilde{z})\sigma T^4(\tilde{z}) - \varepsilon(\tilde{z})\sigma\int_{\tilde{\eta}} T^4(\tilde{\eta})\,dF_{\tilde{z}-\tilde{\eta}} + \varepsilon(\tilde{z})\int_{\tilde{\eta}}\frac{1-\varepsilon(\tilde{\eta})}{\varepsilon(\tilde{\eta})}Q_L(\tilde{\eta})\,dF_{\tilde{z}-\tilde{\eta}} - Q(\tilde{z}) \quad (16)$$

where $\tilde{z}$ is the axial coordinate of the sample point considered, $Q(\tilde{z})$ is the irradiation profile generated by the lamp, the integrals extend over the sample,

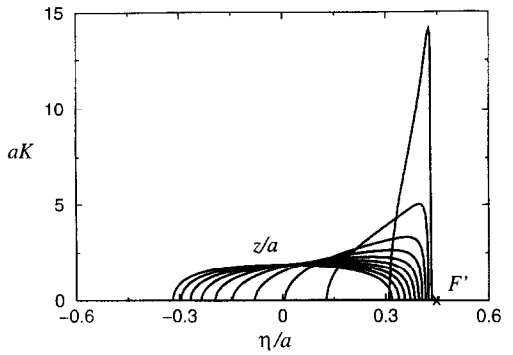

Fig. 3. View factor kernel. Curves correspond to negative values of z.

and $dF_{z-\tilde{\eta}}$ is the view factor between two infinitesimal elements. Notice that the non-reflection model is obtained from the previous equation if the integral terms are eliminated.

The determination of the view factor is just a geometrical problem (see refs. [14, 15]). In the simplified 1D model that we are considering, the totality of the radiation that leaves a sample ring (actually, a sample point) which arrives at another sample ring, is reflected at the same ellipsoid ring. This means that the view factor between the two sample rings is the same as that between one sample ring and the furnace ring. The calculation of this view factor is presented in the Appendix, equations (A8) and (A10); it can be expressed as (notice the change in nomenclature)

$$dF_{z-\eta} = K(z,\eta)\,d\eta \tag{17}$$

where $z = \tilde{z}/a$ and $\eta = \tilde{\eta}/a$ represent axial coordinates in a system with origin in the center of the ellipsoid. The kernel $K(z,\eta)$ [equation (A10)] is represented in Fig. 3 where the function $K(\eta)$ is plotted for fixed negative values of z (for positive values of z one has the figure symmetrical with respect to the center of the ellipsoid). Each curve represents the fraction of radiant energy leaving a fixed point z that arrives after one mirror reflection at a point η in the ellipsoid axis. Since the emitting point is considered between both foci ($z_F < z < z_{F'}$), no energy arrives at points beyond focus $F'(\eta > \eta_{F'})$; there is always, for each value of z, a value of η beyond which the sample (the axis) is not exposed to the redistributed energy. When the radiating point is very close to focus F, there is only a narrow zone close to focus F' affected, as expected.

With respect to the upper base of the cylinder, we are going to consider the following simplified radiative model (non-reflecting)

$$Q_b(\hat{r}) = \varepsilon\sigma(T^4(\hat{r},-L) - T_0^4) - Q_0\left[q_{b1}\left(\frac{\hat{r}}{R}\right) + q_{b2}\left(\frac{\hat{r}}{R}\right)\right] \tag{18}$$

where $q_{b1}(r)$ and $q_{b2}(r)$ are given by equations (8) and (11). This model can be simplified further for a 1D sample as follows

$$\bar{Q}_b = \varepsilon\sigma(\bar{T}^4 - T_0^4) - Q_0(\bar{q}_{b1} + \bar{q}_{b2}) \tag{19}$$

where $\bar{T}$ is the average temperature at the upper base, and $\bar{q}_{b1}$ and $\bar{q}_{b2}$ are the average irradiation profiles at the upper base, that is

$$\bar{q}_{b1} = 2\int_0^1 r q_{b1}(r)\,dr \quad \bar{q}_{b2} = 2\int_0^1 r q_{b2}(r)\,dr \tag{20}$$

which can be easily obtained from equations (8) and (11).

4. TEMPERATURE FIELD IN THE SAMPLE

In order to analyse the behavior of the radiation model just formulated, the temperature field in the cylindrical sample will be calculated. To simplify the problem, a 1D model will be considered (as indicated in ref. [2], the use of a 1D model is appropriate for the case $\Lambda \gg 1$). The numerical results will be presented in Section 5.

The problem is considered to be axisymmetric; thus, only half the diametral section needs to be considered. Here, we consider the cylindrical coordinate system with origin in the center of the cylinder described above. The transfer of energy is given by the conduction equation

$$\frac{\partial^2 T}{\partial \hat{z}^2} + \frac{1}{\hat{r}}\frac{\partial}{\partial \hat{r}}\left(\hat{r}\frac{\partial T}{\partial \hat{r}}\right) = 0 \tag{21}$$

and the following boundary conditions (k being the thermal conductivity)

$$T(\hat{r}, L) = T_b \quad \frac{\partial T}{\partial \hat{r}}(0,\hat{z}) = 0 \tag{22}$$

$$-k\frac{\partial T}{\partial \hat{r}}(R,\hat{z}) = Q_L(\hat{z}, T(R,\hat{z}))$$

$$k\frac{\partial T}{\partial \hat{z}}(\hat{r}, -L) = Q_b(\hat{r}, T(\hat{r}, -L)) \tag{23}$$

that is, the known temperature on the lower base of the cylinder (T_b), symmetry condition at the axis of the cylinder, and energy balance on the lateral surface of the cylinder and on the upper base. In this model heat losses to the surrounding gas (usually Ar or He) are not taken into account. The physical properties of the sample are assumed constant. The function Q_L for 1D samples is defined implicitly by equation (16), and Q_b by equation (18).

4.1. *Dimensionless equations*

The dimensionless temperature is defined as $\theta = T/T_m$, where T_m is the melting temperature, and the dimensionless coordinates as $r = \hat{r}/R$ and $z = \hat{z}/L$. The non-dimensional equations for the model given by equations (21)–(23) are

$$\frac{\partial^2 \theta}{\partial z^2} + \Lambda^2\frac{1}{r}\frac{\partial}{\partial r}\left(r\frac{\partial \theta}{\partial r}\right) = 0 \tag{24}$$

$$\theta(r,1)=\theta_b \quad \frac{\partial\theta}{\partial r}(0,z)=0 \tag{25}$$

$$-\frac{\partial\theta}{\partial r}(1,z)=Raq_L(z,\theta(1,z))$$

$$\frac{\partial\theta}{\partial z}(r-1)=Ra\Lambda q_b(r,\theta(r,-1)) \tag{26}$$

where $\theta_b=T_b/T_m$, Ra is the radiation parameter given by

$$Ra=\frac{\varepsilon\sigma T_m^3 R}{k} \tag{27}$$

and the functions q_L and q_b are defined by

$$Q_L=\varepsilon\sigma T_m^4 q_L \quad Q_b=\varepsilon\sigma T_m^4 q_b. \tag{28}$$

4.2. *One-dimensional model*

Let us define a radially-averaged temperature as

$$\bar{\theta}(z)=2\int_0^1 \theta(r,z)r\,dr \tag{29}$$

then from equation (24), and using the boundary conditions one obtains the following approximate equation ($\theta(1,z)\approx\bar{\theta}(z)$)

$$\frac{d^2\bar{\theta}}{dz^2}=2\Lambda^2 Raq_L(z,\bar{\theta}) \tag{30}$$

which must be integrated with the boundary conditions ($\theta(r,-1)\approx\bar{\theta}(-1)$)

$$\bar{\theta}(1)=\theta_b \quad \frac{d\bar{\theta}}{dz}(-1)=Ra\Lambda\bar{q}_b(\bar{\theta}(-1)). \tag{31}$$

The function $q_L(z,\bar{\theta})$ is obtained from equation (16) which, after taking ε constant for simplicity, reads

$$q_L(z)=\bar{\theta}^4(z)-\int_\eta \bar{\theta}^4(\eta)K(z,\eta)\,d\eta$$

$$+(1-\varepsilon)\int_\eta q_L(\eta)K(z,\eta)\,d\eta-P_W q(z) \tag{32}$$

where P_W is the dimensionless power parameter given by

$$P_W=\frac{Q_0}{\varepsilon\sigma T_m^4} \tag{33}$$

and the irradiation profile $q(z)$ is given by equation (6). The function $\bar{q}_b(\bar{\theta}(-1))$ is obtained from equation (19)

$$\bar{q}_b=[\bar{\theta}(-1)^4-\theta_0^4]-P_W(\bar{q}_{b1}+\bar{q}_{b2}) \tag{34}$$

where the profiles $\bar{q}_{b1}$ and $\bar{q}_{b2}$ are given by equation (20), and $\theta_0=T_0/T_m$.

4.3. *Numerical procedure*

The temperature distribution, $\bar{\theta}(z)$, is obtained numerically. From now on the bar in $\bar{\theta}$ is dropped for simplicity. We define $F(\theta)=\theta^3$, so that equation (30) can be cast in the form

$$\frac{d^2\theta}{dz^2}-2\Lambda^2 RaF(\theta)\theta=2\Lambda^2 Raq_L^*(z,\theta) \tag{35}$$

where $q_L^*=q_L-F(\theta)\theta$. We find this formulation more adequate for the numerical procedure used to solve it.

The nonlinear equation (35) is solved using an iterative scheme, where at each step the following linearized problem is solved:

$$\frac{d^2\theta}{dz^2}-2\Lambda^2 RaF(\tilde{\theta})\theta=2\Lambda^2 Raq_L^*(z,\tilde{\theta}) \tag{36}$$

$$\theta(1)=\theta_b \quad \frac{d\theta}{dz}(-1)=\Lambda Ra\bar{q}_b(\tilde{\theta}(-1)) \tag{37}$$

where $\tilde{\theta}(z)$ represents the known temperature at the previous step. This second-order, linear, ordinary differential equation is solved using standard finite difference methods. The iteration process is started considering $\theta=\theta_b$ as the initial step, and it is stopped when

$$\frac{\sum_i|\theta_i-\tilde{\theta}_i|}{\sum_i|\theta_i|}<10^{-5}. \tag{38}$$

At each step the function $q_L(z,\tilde{\theta})$ is obtained from equation (32) by iteration, starting with $q_L(z)=0$ (the iterative scheme is described in some detail in ref. [16]).

5. RESULTS

The results presented in this section have been obtained for a silicon sample. The physical properties of Si [9] and the geometrical and furnace operations parameters used in this section are the following

$T_m=1690\,K$ $\quad a=90\times10^{-3}\,m$

$k=22\,W\,m^{-1}\,K^{-1}$ $\quad b=80\times10^{-3}\,m$

$\varepsilon=0.7$ $\quad 2L=80\times10^{-3}\,m$

$2R=8\times10^{-3}\,m$ $\quad T_0=400\,K$

$T_b=800\,K$

$W_L=400$ W (except when the dependence on W_L is studied).

For these values the radiation parameter [equation (27)] takes on the value $Ra=0.035$, and the power parameter [equation (33)] the value $P_W=4.3$.

The temperature distribution $\theta(z)$ is presented in Fig. 4(a) for different sample positions (different values of d). In Fig. 4(b) we also present the temperature distribution obtained when the non-reflection model is considered. One can see that for small values of d the differences between them are small: just a slight increase in temperature in the top part

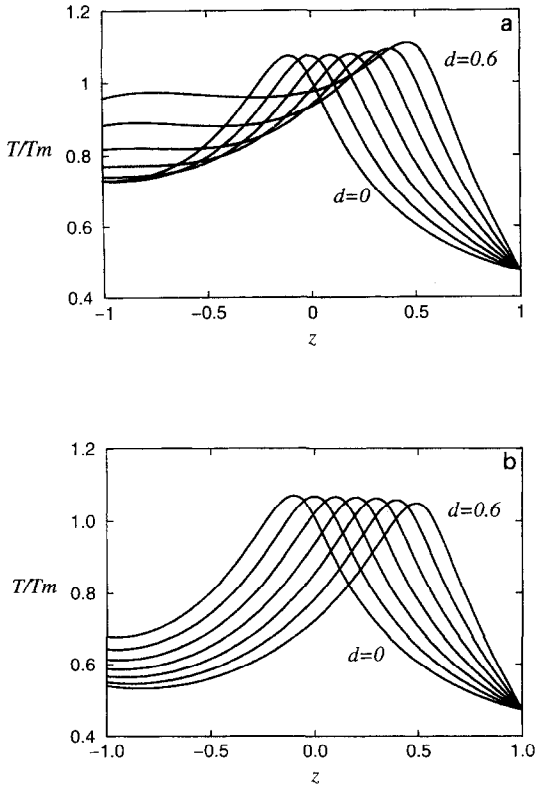

Fig. 4. Temperature distribution for different sample positions: (a) reflection model; (b) non-reflection model. Curves correspond to $d = 0, 0.1, 0.2, 0.3, 0.4, 0.5$ and 0.6.

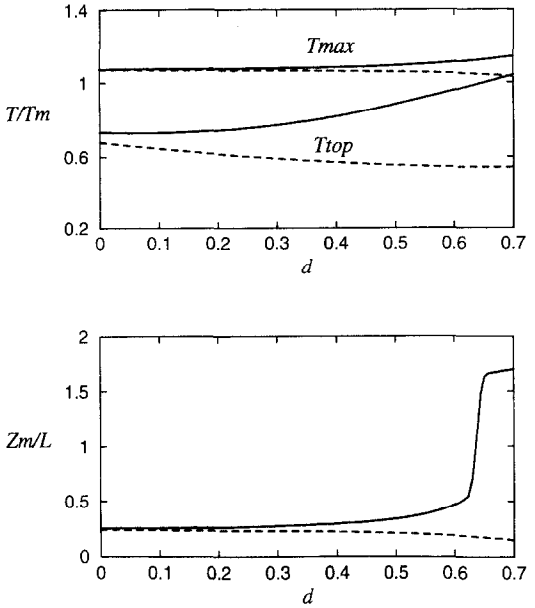

Fig. 5. Variation with the sample positioning, d, of the maximum temperature, T_{max}, the upper-base temperature, T_{top} and the molten length, Z_m. $W_L = 400$ W. —, reflection model; – – –, non-reflection model.

of the sample. However, for large values of d the temperature fields obtained with both models are quite different: in the reflection model the maximum temperature is higher, and the temperature distribution is quite asymmetric. The dependence with d of the maximum temperature, T_{max}, the upper-base temperature, T_{top}, and the volume of melt (the length of melt in our one-dimensional model, defined as the length of the interval where $\theta(z) > 1$), Z_m, are presented in Fig. 5. In the non-reflection model T_{max}, T_{top} and Z_m decrease slightly with d; however in the reflection model they increase with d, T_{max} increases slightly and T_{top} and Z_m do so more strongly. In fact, for $d \approx 0.63$, the top of the sample melts, as indicated by the jump in the figure for Z_m. The difference between the reflection and non-reflection models gets stronger as d increases.

Our model also predicts the necessary lamp power for furnace operation. It is clear that if we aim at having a constant molten zone we will require less power in the reflection model. If we chose the value $Z_m = 0.3L$ (this corresponds to a molten zone of 12 mm) we would obtain the operation diagram shown in Fig. 6. The pulling of the rod takes place in practice very slowly. We can imagine a quasi-stationary process where the pulling is simulated by decreasing the value of d. We see from Fig. 6 that in the reflection model the pulling must be accompanied by an increase in lamp power. Notice that the non-reflection model does not reproduce the previous trend: the lamp power remains fairly constant, and always higher than the power required in the reflection model.

5.1. *Comparison with experiments*

Our results are now compared with experimental data [17] (part of which are published in [18]) that consists in the temperature distribution measured along the surface of a Si sample of 7.6 mm in diameter and 90 mm in length in an Argon atmosphere of 1300 mbar with a lamp power of 510 W. The molten zone obtained is 13 mm long. In order to define the physical parameters for our simplified model, the following considerations are made.

(a) An analysis of the influence of the atmosphere that surrounds the sample is made in [19]. It is shown that the temperature measured in a graphite sample in an atmosphere $\approx 10^3$ mbar is $\approx 20\%$ lower than that measured in vacuum ($\approx 10^{-5}$ mbar): the

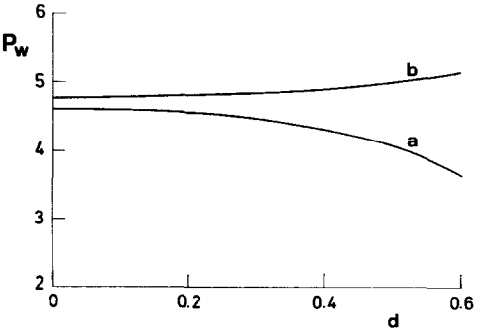

Fig. 6. Operation diagram for having constant molten length. $Z_m = 0.3\,L$: (a) reflection model; (b) non-reflection model.

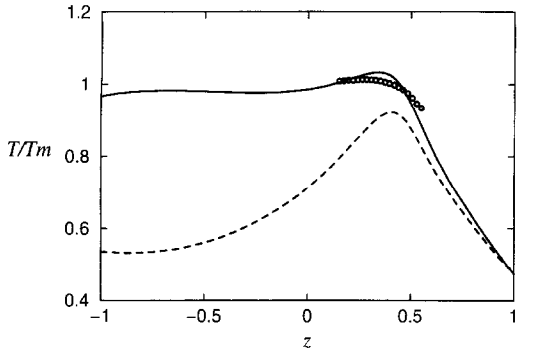

Fig. 7. Comparison with experimental results. —, Reflection model; – – –, non-reflection model; ○, experimental data.

maximum temperature decreases from 1093 K or 873 K. Or, the other way around, to obtain approximately the same maximum temperature, a reduction in power of $\approx 40\%$ must be made; the decrease goes from 166 W with $\approx 10^3$ mbar to 100 W with $\approx 10^{-5}$ mbar. Since our model does not include the effect of the external atmosphere, we will consider a power reduction of 40% with respect to the 510 W used in the experiment. Thus, in our model we will consider a power of 306 W.

(b) In an actual run the sample is translated ≈ 20–25 mm (see [18]). In the ellipsoid used (of semiaxes 90/80) the distance between the center of the ellipsoid and the focus is 41 mm, thus a sample 90 mm long can go into the second half of the ellipsoid a maximum distance of ≈ 30–35 mm. In our model we will consider a representative value of 26.5 mm, thus the distance between the center of the sample and the focus, $\hat{d}$, will be 22.5 mm and hence our dimensionless parameter will be $d = 0.5$.

(c) In our model the physical properties of the sample are assumed constant. We must used representative values for the thermal conductivity, k, and the emissivity, ε. We will consider weighted averages. For solid Si we have the following values of k (in W m^{-1} K^{-1}): 42 at 800 K, 31 at 1000 K, 26 at 1200 K, 22 at 1600 K; and for liquid Si, 67 at 1700 K. A weighted average considering a typical temperature profile and 13 mm of molten zone is $k = 33$ W m^{-1} K^{-1}. With respect to ε we only have the values for solid and liquid Si, 0.7 and 0.3, respectively, thus we will consider the weighted average $\varepsilon = 0.64$.

The results obtained with both the reflection and non-reflection models are presented in Fig. 7, along with the experimental data. Since the axial position of the experimental profile (for instance, with respect to the ellipsoid) is not known (see [18]), for convenience, in Fig. 7, it is placed so that the maximum temperatures approximately coincide. The maximum temperature in our reflection model is ≈ 1746 K and the molten length ≈ 14.7 mm as compared to the experimental values, 1705 K and 13 mm; a small error for a very simplified model. On the contrary, the non-reflection model provides a maximum temperature of 1557 K well below the melting temperature. On the other hand, qualitatively, the reflection model reproduces the asymmetric temperature distribution observed experimentally [19]. We conclude that, despite the limitations inherent to our reflection model, it provides accurate results both qualitative and quantitatively.

6. CONCLUSIONS

The heating of a cylindrical slender sample in a monoellipsoidal mirror furnace has been studied. The radiative exchange between the sample and the mirror has been formulated. Since only slender samples are of interest, the assumption of a one-dimensional sample has been made in order to simplify the analysis. In this model the energy radiated by the sample is reflected at the mirror and redistributed along the sample. The purpose of this paper has been the modelling of the radiation problem, thus for simplicity the temperature field has been obtained using a stationary, one-dimensional, constant-property model. The results provided by this approximate model show important qualitative differences with respect to a non-reflection model, where the energy radiated by the sample were just lost.

Comparison with experiments shows a good agreement between the results obtained with the reflection model and the experimental data, whereas the discrepancies between experiment and non-reflection model are large. Also, one of the characteristics of Si-floating-zone crystals grown under microgravity is the asymmetry in the solid–liquid interfaces: as shown by surface topograms [20] the curvature of the feed–rod interface is much steeper than that of the seed–rod interface. (Non-planar interfaces are clearly a result of the thermocapillary flow in the molten zone [21].) In the previous section it was shown [Fig. 4(a)] that in the reflection model the temperature distribution for large values of d was quite asymmetric, and although the conclusions that we can derive from our simplified model must be taken with caution, we point out to this asymmetric heating provided by the furnace as a factor to be considered when analysing the asymmetry in the solid–liquid interfaces.

The radiation model could be improved by considering more than one reflection at the mirror, but that complicates the problem a great deal. Perhaps a different approach, like the Monte Carlo method [14], would render that complicated problem tractable.

Since including the radiative exchange in the model is necessary in order to describe the heating of the sample properly, we propose to combine the one-dimensional radiation model formulated in the present paper, with any other more complete model (two-dimensional, including the material's phase change, the sample's pulling, ...), and thus obtain an accurate model for the melting of a cylindrical sample in a monoellipsoidal mirror furnace.

Acknowledgements—This work has been supported by the Spanish Comisión Interministerial de Ciencia y Tecnología (CICYT) and it is part of a more general endeavour for the study of fluid physics and materials processing under microgravity (Project No. ESP 92-0001-CP). The authors are grateful to Prof. Isidoro Martínez for his help and encouragement, and to Prof. Arne Cröll for his help in providing experimental data.

REFERENCES

1. A. Eyer, R. Nitsche and H. Zimmermann, A double-ellipsoid mirror furnace for zone crystallization experiments in Spacelab, *J. Crystal Growth* **47**, 219–229 (1979).
2. D. Rivas, J. Sanz and C. Vázquez, Temperature field in a cylindrical crystal heated in a mono-ellipsoid mirror furnace, *J. Crystal Growth* **116**, 127–138 (1992).
3. Facilities for microgravity investigations in physical sciences, supported by the ESA, ESA SP-1116 (1989).
4. Experiments facilities for materials and fluids sciences embarked on Spacelab, ESA SP-1120 (1989).
5. K. Kitazawa, K. Nagashima, T. Mizutani, K. Fueki and T. Mukaibo, A new thermal imaging system utilizing a Xe arc lamp and an ellipsoidal mirror for crystallization of refractory oxides, *J. Crystal Growth* **39**, 211–215 (1977).
6. H. G. Riveros, W. K. Cory, R. Toca and E. Camarillo, An ellipsoidal mirror furnace for Czochralski growth, *J. Crystal Growth* **49**, 85–89 (1980).
7. E. R. G. Eckert and E. M. Sparrow, Radiative heat exchange between surfaces with specular reflection, *Int. J. Heat Mass Transfer* **3**, 43–54 (1961).
8. E. M. Sparrow, E. R. G. Eckert and V. K. Jonsson, An enclosure theory for radiative exchange between specular and diffusely reflecting surfaces, *J. Heat Transfer C* **84**, 294–299 (1962).
9. J. L. Duranceau and R. A. Brown, Thermal-capillary analysis of small-scale floating zones: steady-state calculations, *J. Crystal Growth* **75**, 367–389 (1986).
10. J. Zheng, Y. Kamotani and S. Ostrach, 28th Aerospace Science Meeting, AIAA-090-0318 (1990).
11. B. Xiong, Z. M. Tang and W. R. Hu, Thermocapillary convection with phase change in the floating zone under microgravity, *Microgravity Sci. Technol.* **VI**, 131–136 (1993).
12. I. Martínez and A. Cröll, Liquid bridges and floating zones, ESA SP-333, pp. 135–142 (1992).
13. D. Langbein and H. J. Settler, Temperature distribution within a sample in the mirror furnace ELLI in dependence on lamp and sample positions, Technical Report BF-R-65.858, ESTEC, ESA (1984).
14. R. Siegel and J. R. Howell, *Thermal Radiation Heat Transfer* (3rd Edn). Hemisphere, Washington DC (1992).
15. M. F. Modest, Radiative shape factors between differential ring elements on concentric axisymmetric bodies, *J. Thermophysics* **2** (1), 86–88 (1987).
16. E. M. Sparrow, Radiation heat transfer between surfaces. *Adv. Heat Transfer* **2**, 399–452 (1965).
17. A. Cröll, Private communication (1996).
18. A. Cröll, W. Müller-Sebert, K. W. Benz and R. Nitsche, Natural and thermocapillary convection in partially confined silicon melt zones, *Microgravity Sci. Technol.* **III**, 204–215 (1991).
19. P. Dold, Einflüsse statischer und dynamischer Magnetfelder bei der Kristallzüchtung aus Metall- und Halbleiterschmelzen, Ph.D. Thesis, Albert-Ludwigs-Universität, Freiburg (1994).
20. A. Cröll, P. Dold and K. W. Benz, Segregation in Si floating-zone crystals grown under microgravity and in a magnetic field, *J. Crystal Growth* **137**, 95–101 (1994).
21. C. W. Lan and S. Kou, Thermocapillary flow and melt–solid interfaces in floating zone crystal growth under microgravity, *J. Crystal Growth* **102**, 1043–1058 (1990).

APPENDIX

The diffuse view factor between two infinitesimal surfaces dA_1^* and dA_2^* [as shown in Fig. A1(a)] is defined as follows (see [14])

$$dF_{dA_1^*-dA_2^*}=\frac{\cos\phi_1\cos\phi_2}{\pi r^2}dA_2^*=\frac{(\bar{n}_1\cdot\bar{r})(\bar{n}_2\cdot\bar{r})}{\pi r^4}dA_2^*. \tag{A1}$$

We consider the coordinate system shown in Fig. A1(a) whose origin is in the center of the ellipsoid. From this figure we have $\bar{r}_1=(0,r_0,z_0)$, $\bar{r}_2=(R\sin\theta,R\cos\theta,z)$ and, thus, $\bar{r}=\bar{r}_2-\bar{r}_1=(R\sin\theta,R\cos\theta-r_0,z-z_0)$, where r_0 is the radius of the cylindrical sample. The normal unit vectors, $\bar{n}_1$ and $\bar{n}_2$, are given by

$$\bar{n}_1=(0,1,0)\quad \bar{n}_2=\frac{1}{\sqrt{\frac{R^2}{b^4}+\frac{z^2}{a^4}}}\left(\frac{R\sin\theta}{b^2},\frac{R\cos\theta}{b^2},\frac{z}{a^2}\right).$$

The infinitesimal surface dA_2^* is given by

$$dA_2^*=R\,ds\,d\theta=\sqrt{1+\frac{b^4}{a^4}\frac{z^2}{R^2}}dz.$$

Therefore one finally obtains

$$dF_{dA_1^*-dA_2^*}=\frac{(R\cos\theta-r_0)\left(1-\frac{Rr_0\cos\theta}{b^2}-\frac{zz_0}{a^2}\right)b^2}{\pi[R^2+r_0^2-2Rr_0\cos\theta+(z-z_0)^2]^2}d\theta\,dz. \tag{A2}$$

The view factor for the whole furnace ring is given by

$$dF_{dA_1^*-dA_2}=\int_{-\theta_1}^{\theta_1}dF_{dA_1^*-dA_2^*} \tag{A3}$$

where $\theta_1=\arccos r_0/R$ [see Fig. A1(b)].

The view factor $dF_{dA_1^*-dA_2}$ gives the fraction of energy leaving the surface element dA_1^* that arrives at the furnace ring. Because of the axisymmetry of the problem, this view factor is the same for all elements dA_1^* on the sample ring, therefore

$$dF_{dA_1-dA_2}=dF_{dA_1^*-dA_2}. \tag{A4}$$

In our model (slender cylinders) the radius of the sample is infinitesimally small ($r_0\ll R$), thus in the limit $r_0/R\to 0$ we obtain from equation (A2)

$$dF_{dA_1^*-dA_2^*}=\frac{R\cos\theta\left(1-\frac{zz_0}{a^2}\right)b^2}{\pi[R^2+(z-z_0)^2]^2}d\theta\,dz \tag{A5}$$

and from equations (A3)–(A5)

$$dF_{dA_1-dA_2}=\int_{-\pi/2}^{\pi/2}dF_{dA_1^*-dA_2^*}=\frac{2R(a^2-zz_0)b^2}{\pi[R^2+(z-z_0)^2]^2a^2}dz \tag{A6}$$

which can also be written as

$$dF_{z_0-z}=K'(z_0,z)\,dz. \tag{A7}$$

The view factor we are searching can be written as

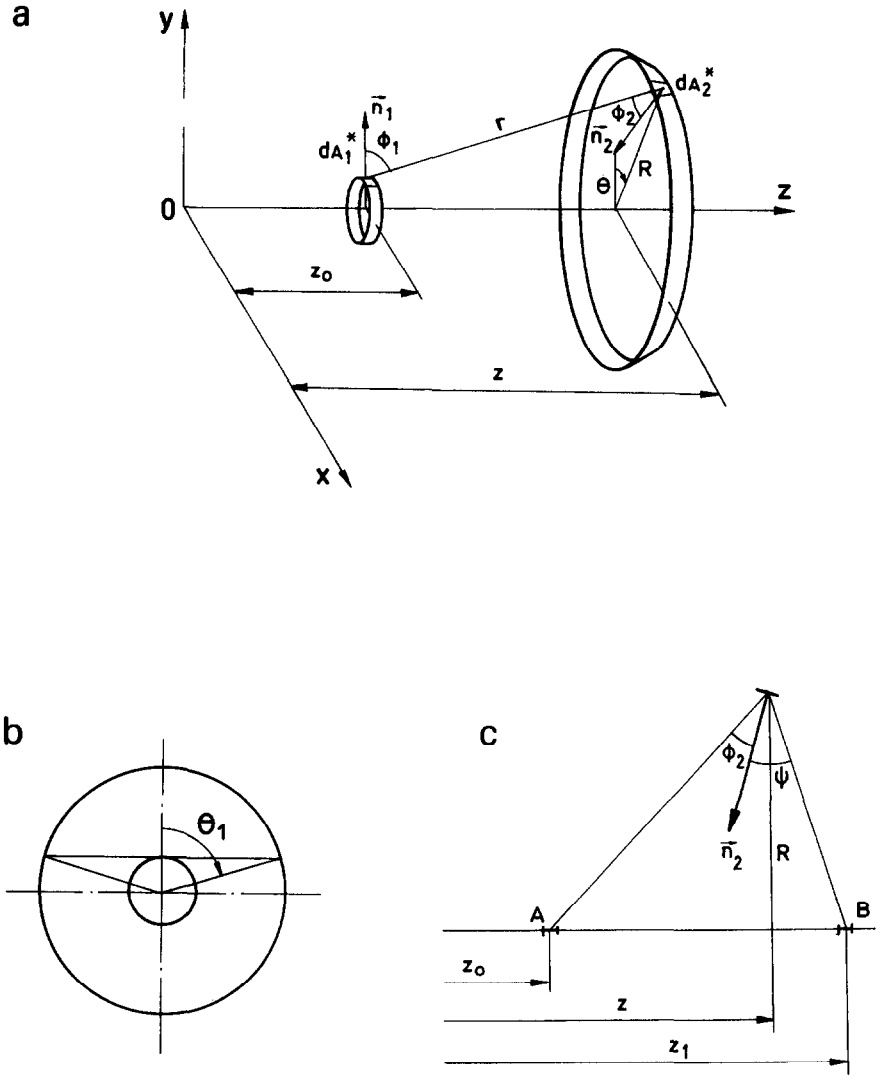

Fig. A1. (a) View factor geometry; (b) definition of θ_1; (c) reflection geometry.

$$dF_{z_0-z_1} = K(z_0, z_1)\,dz_1 \tag{A8}$$

where z_0 and z_1 are the coordinates of the sample rings considered A and B [see Fig. A1(c)]. The relationship between z_1 and z is obtained from the reflection condition $\phi_2 = \psi$, or better, $\cos\phi_2 = \cos\psi$. Thus, proceeding as in the beginning of this Appendix,

$$\cos\phi_2 = \frac{(\bar{r}_2 - \bar{r}_A)\cdot\bar{n}_2}{\|\bar{r}_2 - \bar{r}_A\|} \qquad \bar{r}_A = (0, 0, z_0)$$

$$\cos\psi = \frac{(\bar{r}_2 - \bar{r}_B)\cdot\bar{n}_2}{\|\bar{r}_2 - \bar{r}_B\|} \qquad \bar{r}_B = (0, 0, z_1)$$

hence, we obtain

$$\frac{a^2 - zz_0}{\sqrt{(z-z_0)^2 + R^2}} = \frac{a^2 - zz_1}{\sqrt{(z-z_1)^2 + R^2}}$$

with z and R related by the equation of the axial elliptic section.

The previous equation can be stated as a fourth-degree polynomial in the variable z. Two of the roots of this polynomial are $z = \pm a$ (they verify trivially the reflection condition); the other two are given by the following second-degree polynomial

$$z^2(z_0 + z_1)(a^2 - b^2) - 2za^2(a^2 - b^2 + z_0 z_1) + a^4(z_0 + z_1) = 0.$$

From this equation we obtain explicitly the function $z = z(z_0, z_1)$. Therefore, the view factor obtained before, equation (A7), can be written as

$$dF_{z_0-z_1} = K'(z_0, z(z_0, z_1))\frac{\partial z}{\partial z_1}\,dz_1. \tag{A9}$$

Thus, from equations (A8) and (A9), we obtain the Kernel function $K(z_0, z_1)$ as

$$K(z_0, z_1) = K'(z_0, z(z_0, z_1))\frac{\partial z}{\partial z_1}. \tag{A10}$$